Wasit Journal of Engineering Sciences

Journal homepage: https://ejuow.uowasit.edu.iq

Flow Instability of a Liquid Through a Small-Scale Channel During a Flow Evaporation

Rusul K. Edam[1] | Ahmad A. Y.AL-Waaly[1] | Azzam Sabah Hameed[1]

Affiliations
[1] Department of Mechanical Engineering, Wasit University, Kut, Wasit, Iraq

Correspondence
Ahmad A. Y.AL-Waaly,
Department of Mechanical Engineering, Wasit University, Wasit, Iraq
Email: aalwaaly@uowasit.edu.iq

Received
10-June-2022
Revised
24-June-2022
Accepted
28-June-2022
Doi:10.31185/ejuow.Vol10.Iss2.341

Abstract

Finite volume analysis of two-dimensional model has been performed to study of the influence of heat flux and mass flux on two phase heat transfer through microchannel during water flow boiling. The channel dimensions were (5×5××∘0) m^3. The inlet boundary conditions were (1.63, 3.32, 4.9, 6.65, 8.16) kg/m^2s. The supplied heat fluxes were 24.8kW/m^2, 33.2 kW/m^2, 46.13 kW/m^2, 51 $kW/m^2$and 69 kW/m^2 for nucleate boiling while 33.3 kW/m^2, 50 kW/m^2, 66.7 kW/m^2, 83.3 kW/m^2, and 100 kW/m^2 for dryout condition. The inlet temperature was 30°C. It was shown that the highest heat transfer coefficient occurs at beginning of onset of nucleate boiling (ONB) after that the it will drop due the changing of the flow patterns. According to supplied heat flux, the patterns were bubble flow, dispersed bubbles, churn flow, annular flow, and then dry out condition occurs. For the mass flux 1.63kg/m^2s the highest heat transfer coefficient was 9.5 kW/m^2℃ while for the mass flux 8.16 kg/m^2s the highest heat transfer coefficient was 20kW/m^2 ℃. For the mass flux 1.63kg/$m^2.s$ the highest value of vapour quality was 0.09 while for the mass flux 8.16 kg/m^2s the highest value was 0.15. There is a sharp pressure drop when starts to nucleate and the highest value occurs at dryout condition. This study gave an understanding of the heat exchange flow behaviour during water boiling through a single microchannel.

Keywords: water boiling, microchannel, two phase, critical heat flux, instability, numerical simulation.

الخلاصة: تم استخدام العناصر الحجمية العددية لتحيل لدراسة تأثير التدفق الحراري والتدفق الكتلي على انتقال الحرارة لجريان ثنائي الطور في القنوات المايكروية خلال غليان الماء. ابعاد القناة كانت (5×5×60) m^3. الشروط الحدودية للدخول لحالة الجريان للسائل كانت (1.63, 3.32, 4.9, 6.65, 8.16) kg/m^2s. التدفقات الحراري 24.8kW/m^2, 33.2 kW/m^2, 46.13 kW/m^2, 51 $kW/m^2$and 69 kW/m^2 لبدأ الغليان 33.3 kW/m^2, 50 kW/m^2, 66.7 kW/m^2, 83.3 kW/m^2, 100 kW/m^2 لحالة البخار المحمص. درجة حرارة الدخول كانت 30°C. كانت اعلى قيمة لمعامل انتقال الحرارة كانت في بداية الغليان ثم بعد ذلك تنخفض قيمته نتيجة لتغير طبيعة طور الجريان. تبعا لكمية التدفق الحراري المسبطة يتغير شكل الجريان الى الانواع bubble flow, dispersed bubbles, churn flow, annular flow, and then dry out condition. لمعامل التدفق الكتلي 1.63kg/$m^2.s$ كانت اعلى قيمة لمعامل انتقال الحرارة 9.5 kW/m^2℃ بينما للتدفق الكتلي 8.16 kg/m^2s كانت اعلى قيمة هي 20kW/m^2 ℃. للتدفق الكتلي 1.63kg/m^2s كانت نوعية البخار تساوي 0.09 بينما للتدفق الكتلي 8.16 kg/m^2s كانت نوعية البخار تساوي ٠.١٥. هناك هبوط حاد بالضغط في بداية الغليان بينما اعلى قيمة تحدث عندما يتحول السائل الى البخار المحمص.

1. INTRODUCTION

Depending on the heat of vaporization, two phase heat transfer can handle high demands while maintaining superior temperature uniformity across the chip and allows low flow rates. Combining the flow boiling and the

effect of high surface area to volume ratio in the microchannel can increase heat transfer as compared to normal channel and single-phase flow. High heat flux rate $(7.9)\ \mathrm{MW/m^2}$ can be obtained with a single phase cooling of microchannel heat exchanger having a $(98.6\ )\mu m$ hydraulic diameter [1]. Thats could be much higher cooling rate as compared to nominal size which can extract to $(0.2)\ \mathrm{MW/m^2}$ [2]. During water nucleation through a microchannel, the amount of the heat extracted depends on the difference between inlet fluid bulk temperature and surface temperature of the channel. For water nucleation, there are two different inlet temperatures, first subcooling inlet in which the inlet temperature is much lower than liquid saturation bulk temperature. The second inlet temperature is a saturation temperature which is equal to fluid saturation temperature.
Kandlikar (1998)[3] classified subcooled flow heat transfer into three parts: single phase heat prior to the onset nucleate boiling (ONB). At this stage there is no change in heat transfer coefficient because the surface temperature is less than the saturation temperature of the liquid, see Figure 1. The second part starts at point C which is called onset nucleate boiling (ONB). After that, at point H the saturation condition is attained.

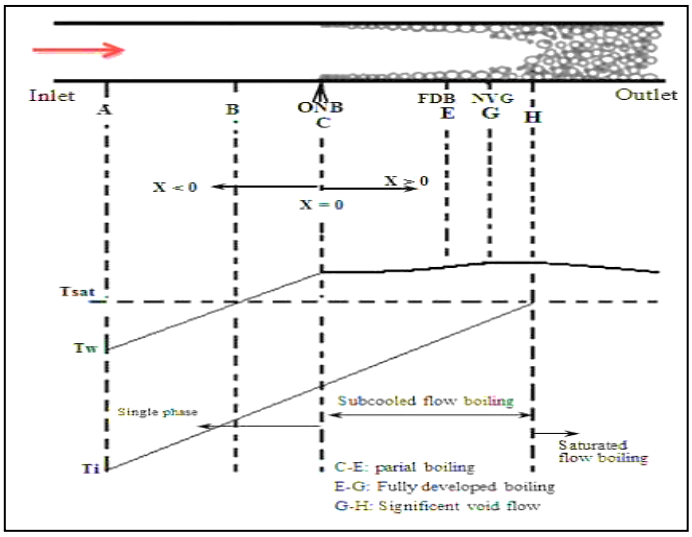

Figure 1 The boiling of a subcooled flow is seen in this diagram, Kandlikar, (1998) [3]

Different two phase flow patterns have been demonstrated by various studies. Jonh and Andrea (2015) [4] presented the most common patterns. These are: bubble flow, annular flow, slug or elongated bubble flow, and mist flow, see Figure 2 and Figure 3. According to their study, the dry zone first developed near the test section's outlet then move upstream toward the inlet with increased in supplied heat flux.

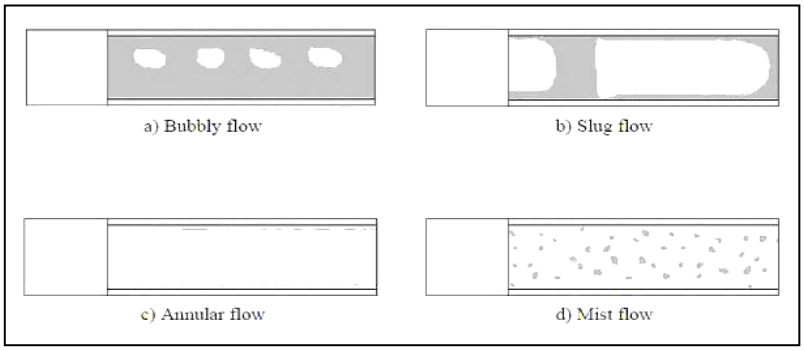

Figure 2 Graphic images of the five primary flow patterns. John and Andrea, (2005)[4]

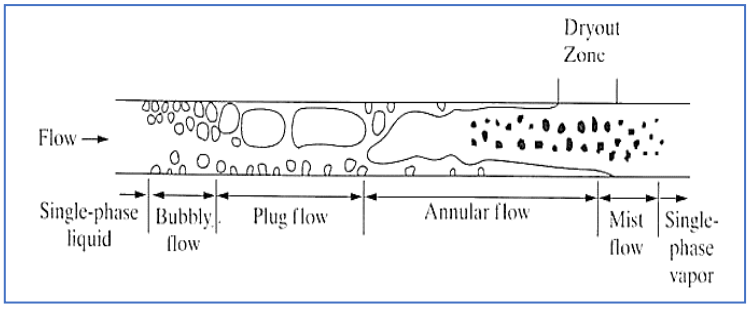

Figure 3 Flow and heat transfer regimes with moderate heat flux Ghiaasiann,(2008)[5]

Qu and Mudawar 2003a[6] found that the coefficient of heat transfer depends on vapour quality and mass flux but independent on heat flux during the convective boiling. While the nucleate boiling is the dominant heat transfer mechanism for water nucleation through the microchannels heat sinks. Both convective and nucleate boiling mechanism described by Lee and Mudawar 2005 [7]. They conducted experiments of the flow boiling heat transfer in a copper microchannel which has a rectangular shape using R134a as working fluid. They found that at high heat flux and vapour quality film boiling was dominant.

Cheol and Moo 2007 [8] found heat transfer coefficient was independent on the heat flux and vapour quality. They demonstrated that the nucleate boiling was the dominant heat transfer mechanism during flow boiling. Soupremanien et al., 2011[9] results proved that pressure drop affected by the aspect ratio of minichannel. Moreover, they showed that the heat transfer coefficient is affected by both hydraulic diameter and aspect ratio of the mini channel. Galvis 2012[10] explained the water flow boiling properties in two different single copper micro channel of different hydraulic diameter but same length and aspect ratio. Two separate inlets subcooling between (50.7 to 54.2)℃ was used. It was shown that the nucleate boiling was predominante heat transfer mechanism for the smaller channel while the convective boiling was dominant upon nucleate boiling. Balasubramanian et al. 2013 [11] performed experimental investigation of flow boiling of water in microchannels over wide range of heat flux up to $140 kW/m^2$ and mass flux up to $88 kg/m^2 s$. The local flow boiling heat transfer coefficient change was depending on the flow boiling regime which was associated with heat transfer mechanism. Moreover, their results showed that the annular flow regime provides the most stable flow boiling regime.

Fayyadh et al. 2017[12] conducted experimental study at range of heat flux (11.46-403.1)kW/m^2 and mass flux (50-300)$kg/m^2 s$. The researchers investigated the flow boiling heat transfer of R134 in copper multi micro channel heat sink consisted of 25 rectangular micro channel, hydraulic diameter $420 \mu m$. Three flow patterns were observed bubble, slug and wave-annular flow.

Yin et al., 2017[13] studied the effect of subcooled inlet and aspect ratio on flow boiling of water through a rectangular microchannel. Test section length was 40mm, hydraulic diameter was $571 \mu m$, aspect ratio was 20 while inlet temperature was 65℃. The key discover is that nucleate boiling dominant heat transmission during flow boiling in micro channel with high aspect ratio.

Kuang et al., 2017[14] studied the pressure drop fluctuation in micro channel evaporator. The model consists of four parallel (1×1.1) mm micro channel with heated length of $250 mm$, ammonia and water as working fluids. Experimental results indicated that the pressure drop fluctuation is type of impulse wave and the wave trough lasts longer than the wave crest.

Al-Nakeeb et al. 2021 [15] used a channel of a hydraulic diameter $420 \mu m$ and length $60 mm$. They investigated that when the mass flux increases the heat transfer coefficient increases. And nucleate boiling and forced convective boiling are dominating as heat transfer mechanism. Özdemir et al., 2021[16] showed that for low and medium heat fluxes, the local heat transfer coefficient increases while the channel aspect ratio had no effect on heat transfer coefficient for larger heat fluxes.

Zhangyu et al. 2017 [17] numerically studied the properties of flow boiling heat transfer in horizontal micro channel. The results presented that heat transfer coefficient increases significantly and then decreases when the degree of evaporation rises. Claesson, 2017[18] studied the transition processes inside microchannel $5 mm$ length and $0.64 mm$ diameter. They decided to use the numerical tools rather than experimental methods to easily investigate the flow inside the microchannels in more thorough and precise manner. There are three stages in the transition from isolated bubble flow to confined bubble flow: sliding, merging also post-merging stages. The results showed the local heat transfer coefficient is enhanced by the coalescence of the annulus and the bubble during the transition from slug to annular flow.

The aim of this study is to investigate the flow behaviour of water nucleation through a microchannel using experimental and numerical analyses. For the numerical analysis a Computational Fluid Dynamics (CFD) using commercial software ANSYS version (21.1). Based on validation of numerical results with experimental results, two-phase flow patterns will be investigated. For a specific channel dimensions, different mass and heat fluxes

will be investigated in order to predict the point of nucleation start(s) and the value of critical heat flux where the flow became unstable turns into totally vapour.

2. Experimental Work

2.1.Test rig description

Figure 4 and Figure 5 show the experimental setup and a schematic description of the flow loop respectively. The reservoir (1) was used to supply distilled water to the test model (5) under the effect of the gravity. Transparent plastic tubes have used to connect the test section to the water tank (2). Nine electric heaters have been used to supply the bottom surface of the channel the required heat flux by using three power supplies (3) (APS-3005D brand, 30 Volt and 5 A, and 220 input voltage, 100-60 Hz with accuracy of regulation is 0.012mV). Each power supply feeds three electric heaters. These heaters were made of ceramic and have size (L7*W5*T1.3) mm, model P070513 and resistance 16~21Ω. A thermal paste was added between the heaters and channel bottom surface to reduce thermal resistance. Seven thermocouples K type were used to measure inlet and outlet temperature (4) and channel bottom surface (7). These thermocouples were connected to a computer via data acquisition system (8) TC08. The pressure of entering and exiting fluids has been measured by a pressure transmitter PCM300 (6) (range -100kPa -250 kPa, accuracy 0.5%FS, 4-20mA output signal). The flow visualization section allows for observation of the behaviour of flow boiling (9).

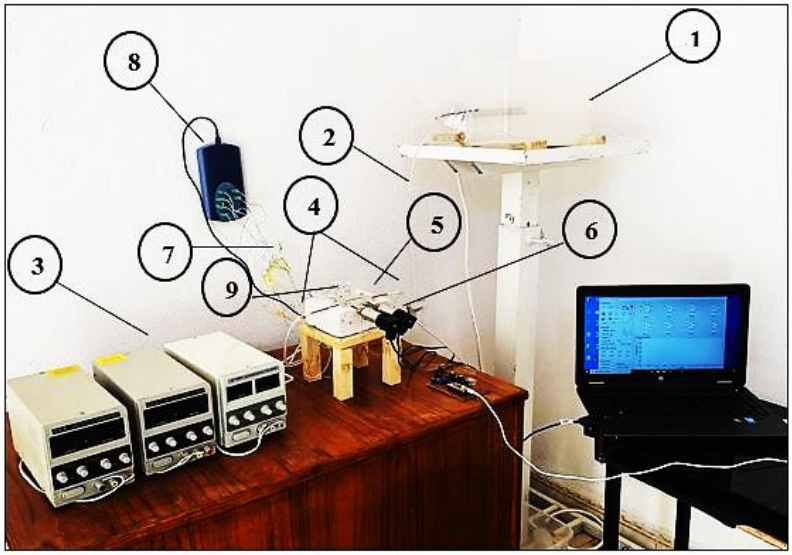

Figure 4 Experimental test rig set-up

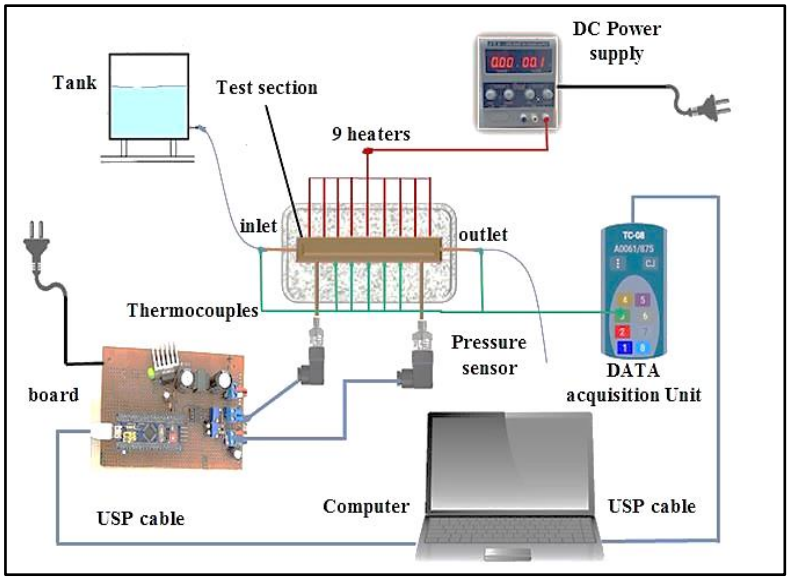

Figure 5 schematic representation of the experimental setup

2.2.Test section

Figure 6 shows a close view of the test section. The test section consists of a mini-channel with dimensions (5mm×5mm×50mm) for the width, height and length respectively and wall thickness of 1mm. The channel was made from a copper metal (specific heat capacity of 380 J/kg K and thermal conductivity of 398 W/m^2K).

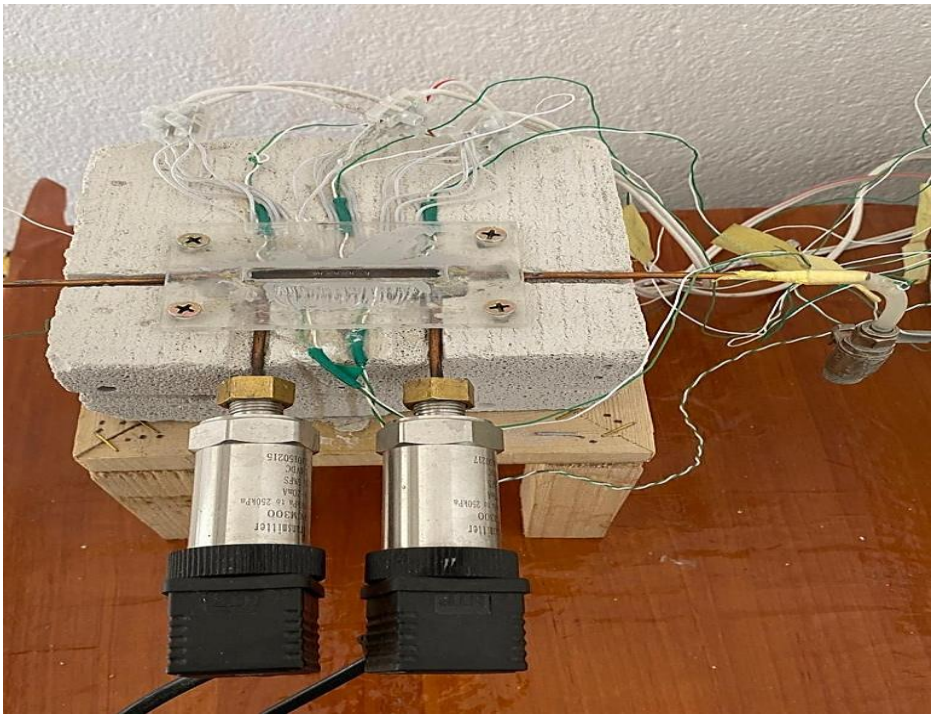

Figure 6 Magnified view of the channel.

The heaters were installed inside a groove with depth 3mm and length 53mm in order to avoid the heat loss, see Figure 7. Moreover, the copper channel was placed above the heaters inside the groove.

Figure 7 Electrical heaters inside the groove in thermiston brick**.**

2.3. Experimental cases

During the experimental five cases were considered in order the investigate the flow boiling behaviour through a horizontal position of the channel, see Table 1. Moreover, Table 1 shows some results of the experimental work where for each mass flux, there are two heat fluxes, the first one where the ware nucleation starts and the other was for onset of dryout.

Table 1 Pressure sensor versus pressure measured in the lab (ρ: density, g: acceleration gravity, h: height)

Cases	Mass flux $kg/m^2.s$	Heat flux (ONB) kW/m^2	Heat flux (Dry out) kW/m^2
CASE1	1.63	24.8	33.3
CASE2	3.32	33.2	50
CASE3	4.9	46.13	66.7
CASE4	6.65	51	83.3
CASE5	8.16	69	100

2.4. Sensors calibration

All of the thermocouples utilized in the present research were pre-calibrated across a distinct temperature range, i.e. from the freezing point of pure water to their boiling point [19]. Furthermore, the pressure sensors were calibrated with five different water heads and ompared with the sensor reading. It was shown that the sensor gives a good agreement with calculated values according to head of the water as shown in Table 2 and Figure 8 below.

Table 2 Pressure sensor versus pressure measured in the lab (ρ: density, g: acceleration gravity, h: height)

P sensor	P = ρgh [kPa]
6	6.46
8	8.6
9	9.8
10.1	10.7
11.3	12.4
12.1	13.2

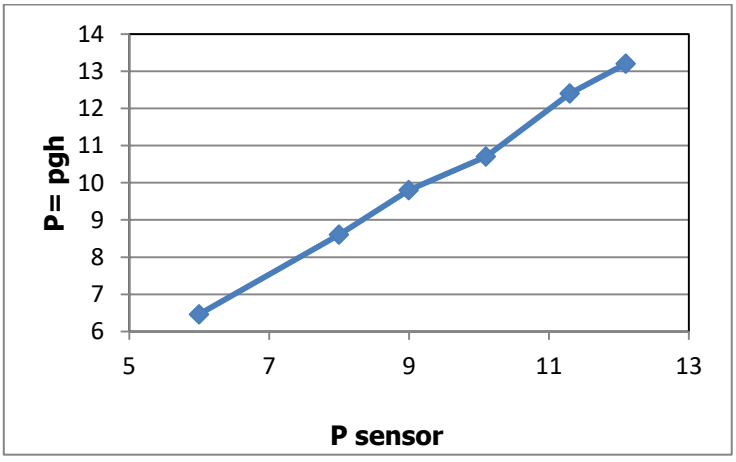

Figure 8 Pressure sensor versus pressure measured in the lab.

2.5. Uncertainty analysis

Uncertainty analysis of a single reading can be calculated by providing three information which are [20]:
B_{xi}, is the bias limit.
$S_{\bar{x}i}$, precision index of the mean.

ν, the number of degrees of freedom (no of readings).
Then, the uncertainty is calculated from

$$U_{95} = [(B_{xi})^2 + (tS_{\bar{x}\imath})^2]^{1/2} \quad (1)$$

$S_{\bar{x}\imath}$ is calculated from

$$S_{\bar{x}\imath} = \frac{S_{xi}}{N} \quad (2)$$

$$S_{xi} = \left\{\sum_{i=1}^{N} \frac{(X_i - \bar{X}_i)^2}{N-1}\right\}^{1/2} \quad (3)$$

Where t is the student multiplier for 95% confidence for the t value. Therefore, the uncertainty in pressure sensor analysis and thermocouple was ±0.232 kPa and ±0.2^{o}C.

3. Finite volume analysis

Computational Fluid Dynamics (CFD) studies are performed using a commercial software ANSYS version (21.1). In order to clarify the influence of the turbulence model which involves the solution of two transport equation, $(k-\varepsilon)$ model and volume of fluid (VOF). Therefore, the techniques of the numerical solution will solve this in Cartesian coordinate system (x, y). Water was chosen as a working liquid and two-dimensional model has been considered and the following assumptions have been adopted: transient flow, two dimensional, Newtonian, incompressible flow, and turbulent.

3.1.Model numerical settings

3.1.1.Model settings

In commercial software ANSYS version (21.1) model settings a multiphase- volume of fluid was used with. The settings of the model were as follows:
Solution method for pressure velocity coupling was: scheme SIMPLE, spatial discretization: for the momentum was *second order upwind*, volume fraction was *compressive*, turbulent kinetic energy was *first order upwind*, turbulent dissipation rate was *first order upwind*, energy was *second order upwind*, transient formulation was *first order implicit*.
Solution controls-under relaxation factors: pressure=0.3, density=1, body force=1, momentum=0.7, vaporization mass=1, volume fraction=0.5, turbulent kinetic energy=0.8, turbulent dissipation rate=0.8, turbulent viscosity=1, energy=1.
Convergence criteria for continuity, x-velocity, y-velocity, energy, k-epsilon was 10-6. Time step was 0.1s, maximum iteration for each time step is 200, transient model, volume fraction cut off equal to 10-6 and courant number 0.25, k-epsilon-realizable, near wall treatment-enhanced wall treatment with taking into consideration thermal effect and viscous heating, turbulent intensity was 3%. The boundary conditions were mentioned in section 3.5.

3.2.Governing Equations:[21]

Mass Conservation (Continuity)

The contribution to the mass source for phase p in a cell is

$$\mathrm{m_p} = -\mathrm{m_{p'q^j}} \quad (4)$$

and for phase q is $\mathrm{m_q} = \mathrm{m_{p^i q^j}}$

Momentum Equation

The momentum equation is related to the volume fractions of all phases through the density ρ and dynamic viscosity μ.

$$\frac{\partial}{\partial \mathrm{t}}(\rho\vec{\mathrm{v}}) + \nabla\cdot(\rho\vec{\mathrm{v}}\vec{\mathrm{v}}) = -\nabla \mathrm{p} + \nabla\cdot\left[\mu\left(\nabla\vec{\mathrm{v}} + \nabla\vec{\mathrm{v}}^{\mathrm{T}}\right)\right] + \rho\vec{\mathrm{g}} + \vec{\mathrm{F}} \quad (5)$$

Energy equation

The energy equation will be shared between the phases, is shown below.

$$\frac{\partial}{\partial t}(\rho E) + \nabla \cdot \left(\vec{v}(\rho E + p)\right) = \nabla \cdot \left(k_{eff}\nabla T - \sum_q \sum_j h_{j,q}\vec{J}_{j,q} + (\bar{\bar{\tau}}_{eff} \cdot \vec{v})\right) + S_h \quad (6)$$

k_{eff} is the effective conductivity, $\vec{J}_j$ is the diffusion flux of species j, $h_{j,q}$ is enthalpy of species j in phase q, and $\vec{J}_{j,q}$ is diffusive flux of species j in phase q. The first three terms on the right-hand side is heat transfer due to, species diffusion, and viscous dissipation, respectively. S_h is related to volumetric heat sources that should be defined but not the heat sources created by volumetric of finite-rate or surface interactions because the species enthalpy of formation is already calculated in the total enthalpy calculation as defined in Energy Sources Due to Reaction.

The VOF model treats energy, E, as a mass-averaged variable:

$$E = \frac{\sum_{q=1}^{n} \alpha_q \rho_q E_q}{\sum_{q=1}^{n} \alpha_q \rho_q} \quad (7)$$

$$E_q = h_q - \frac{p}{\rho_q} + \frac{v^2}{2} \quad (8)$$

where h_q for each phase is based on the shared temperature and specific heat of that phase. The properties ρ, k_{eff} and μ_{eff} are calculated by volumetric averaging over the phases. S_h includes the contributions from radiation or any other sources of the volumetric heat.

3.3.System Geometry

The geometry of the system shown in Figure 9 consists of a horizontal channel of square cross-section with a height of 5 mm, a width of 5 mm, and a length of 50 mm, where the lower surface is exposed to heat flux.

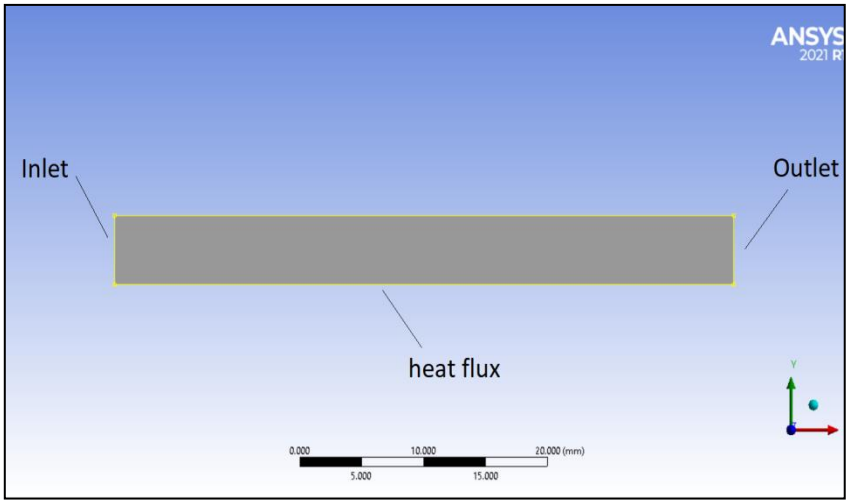

Figure 9 Numerical two dimensional geometry.

3.4.Mesh independency

Mesh independency was checked for the outlet temperature as shown in Table 3. To make a mesh hierarchy, the mesh dependency must be used to find out the correct number of mesh elements that give a stable result that does not change with the change in the size of the mesh. Figure 10 shows the test of the number the mesh elements.

Table 3 Mesh independency.

case	No. mesh of Element	Fluid outlet temperature (^{O}C)
1	15135	95.7
2	20254	97.4
3	23214	98.2
4	25050	98.3

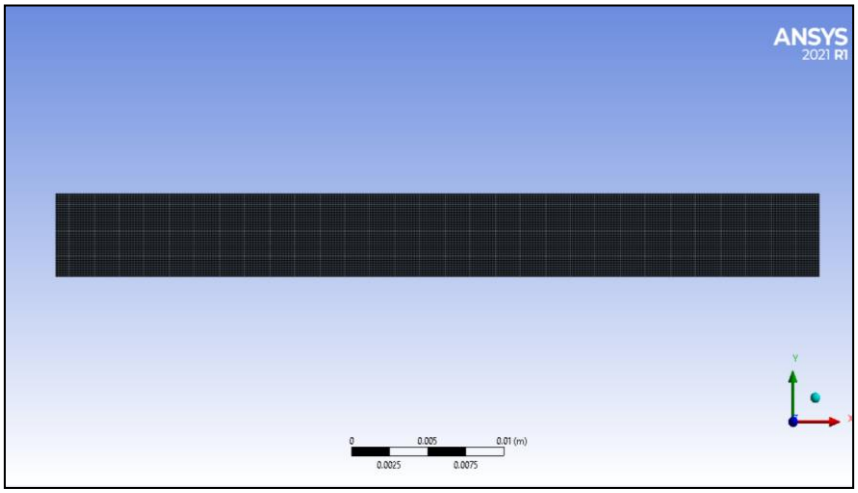

Figure 10 Structure mesh generated**.**

3.5. Conditions of the Boundary

Five cases were tested, five mass fluxes cases (0.1, 0.15, 0.2, 0.25) m/s. For each mass flux there was a specific heat flux where the water nucleation starts and the other for the dry out conditions, see Table 1. The temperature of the entry area was 30 degrees Celsius and in the exit area the pressure was 0Pa.

4. RESULTS AND DISCUSSION

4.1. Numerical results validation

A comparison between the numerical and experimental results were performed. Based on good agreement between these results, the rest of the analysis will be based on numerical analysis. Two parameters have been considered for the validation, two phase flow patterns and channel bottom wall temperature. It is important to mention here that the pressure measurement will not considered for the validation that is due to the low accuracy of the pressure sensors (about 1 kPa). Pressure drop through the channel will be lower than the resolution of the pressure sensor, therefore, the sensors can't detect the pressure drop through the channel.

4.1.1. Two phase flow patterns

Figure 12 shows a sequential progress of the flow patterns for both numerical and experimental results. The flow starts with bubbles flow, dispersed flow, churn flow, and annular flow. The nucleation starts at 69 kW/m^2. After that the flow turned dry out conditions because of the heat flux reached to the critical value which in this case equal to 100 kW/m^2. The other values of mass and heat fluxes are shown similar behaviours. Figure 12 shows a good agreement between the numerical and experimental results. The deviation can be justified because the numerical analysis considered a two-dimensional model while the experimental was an actual three dimensional model.

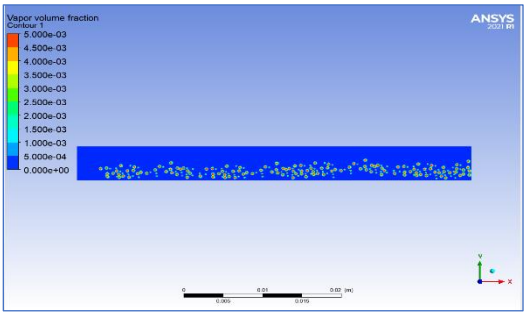

(a) Bubble flow

Figure 11 (continued)

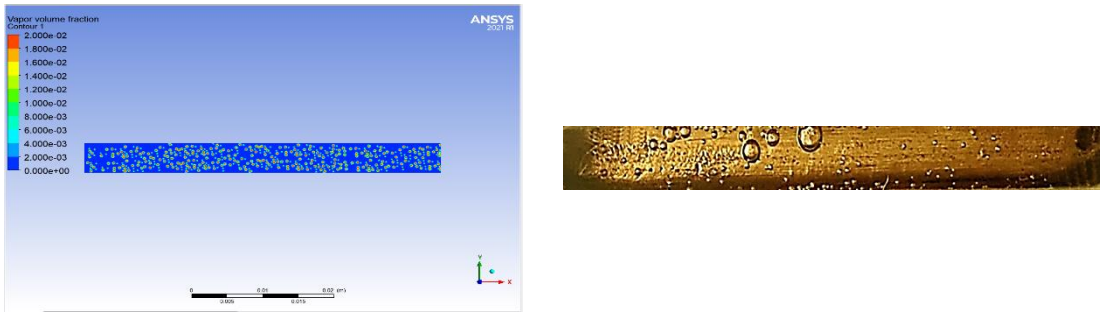

(b) Dispersed bubble

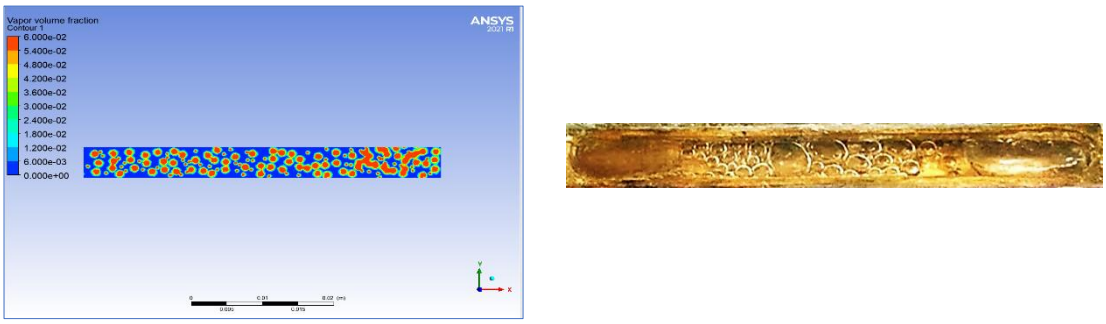

(c) Churn flow

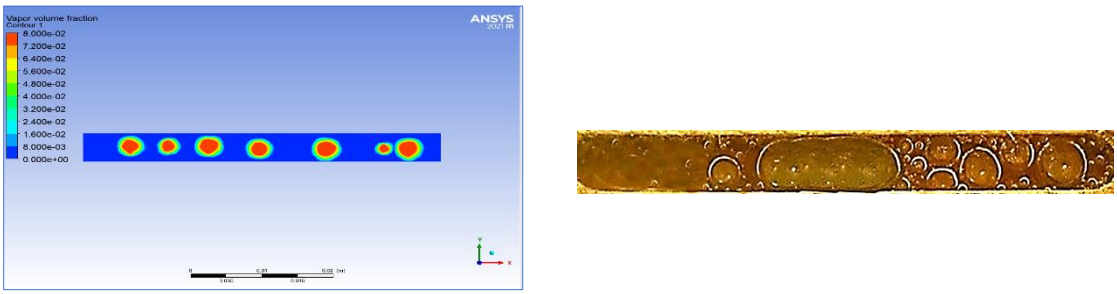

(d)Annular flow

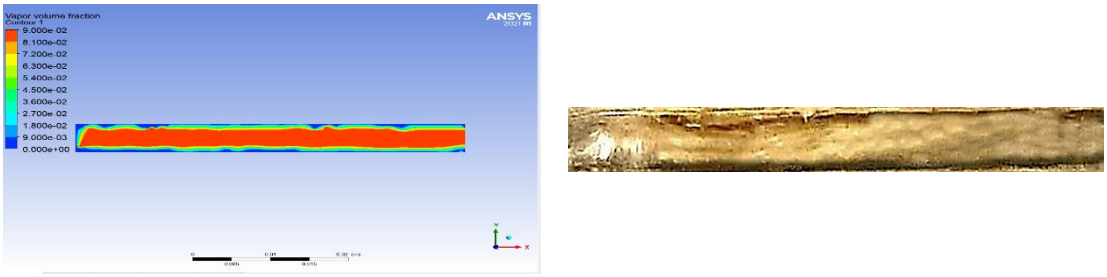

(e) Dry out

Figure 12 A comparison flow pattern between numerical work and experimental work, case five with mass flux 8.16kg/$m^2 s$ where nucleation start at 69kw/$m^2$and dry out occur at 100kw/m^2

4.1.2. Channel bottom wall temperature

Figure 13 a comparison between numerical and experimental results for the channel bottom wall temperature. It is shown that there is a good agreement between the values of the wall temperature for the numerical and experimental results. It was obvious that there is a small deviation between both results because that the numerical results based on a two-dimensional model. Therefore, the numerical analysis can't predict the behaviour along the third dimension. Figure 13 shows a fluctuation in the wall temperature at the end value of each mass flux, that's due to the effect of dry out conditions, see section 3.3.

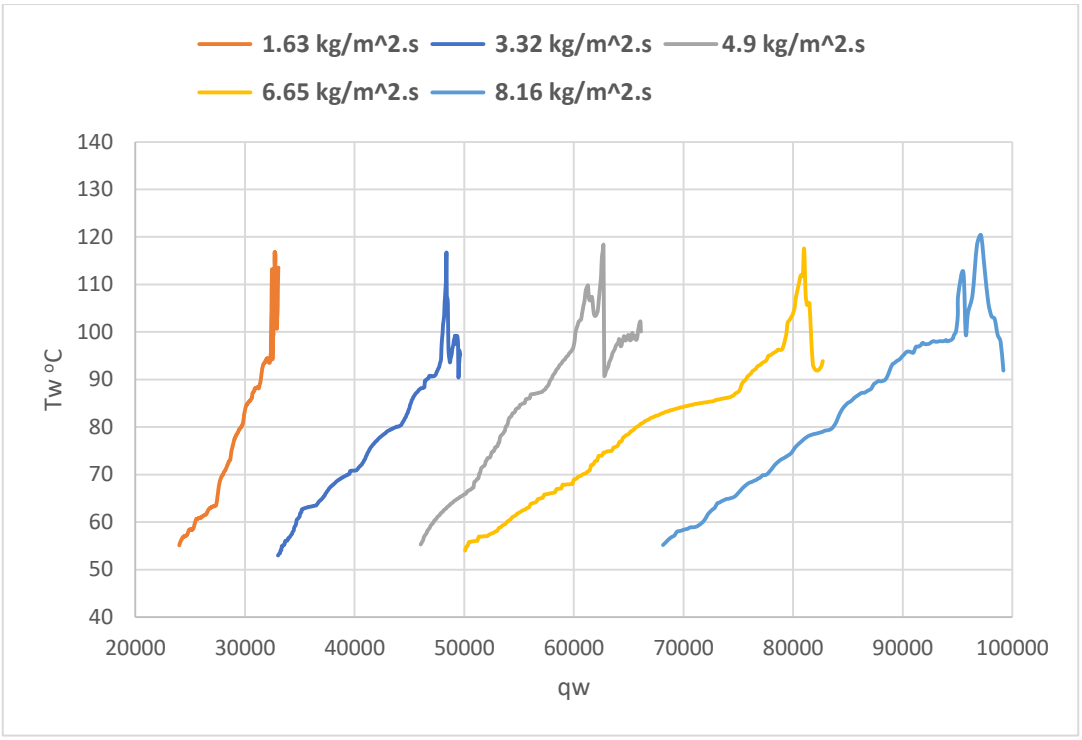

(a) Experimental results

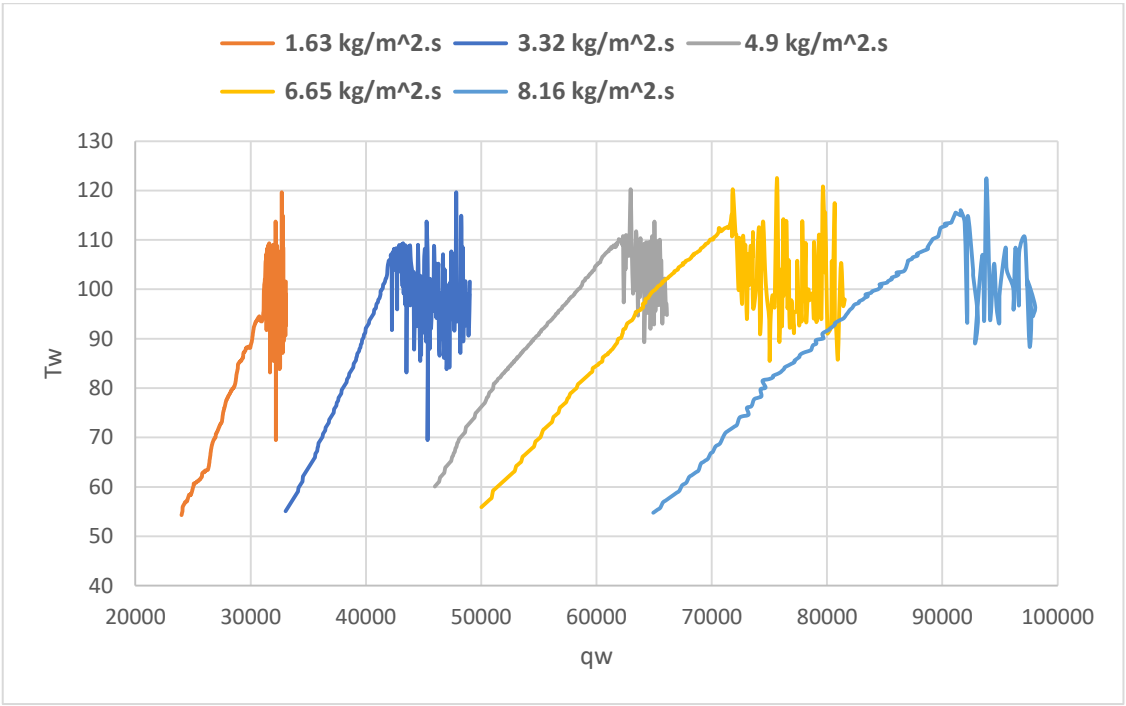

(b) Numerical results

Figure 13 Wall temperature with heat flux of experimental and numerical results.

4.2. Heat transfer coefficient

The following results will be based solely on numerical analysis because there was a good agreement between the numerical and experimental results, see section 4.1.

4.2.1. Effect of heat flux

For given a heat flux input the heat transfer coefficient is high at (ONB), possibly due to the beginning of the two phase boiling. The ONB induces a fast releases of latent heat of water and reduces the high temperature of the wall that available prior to ONB. From Figure 14 we noted that the highest heat transfer coefficient in the case five at mass flux 8.16 kg/$m^2.s$ where it reaches 20kW/m^2℃.

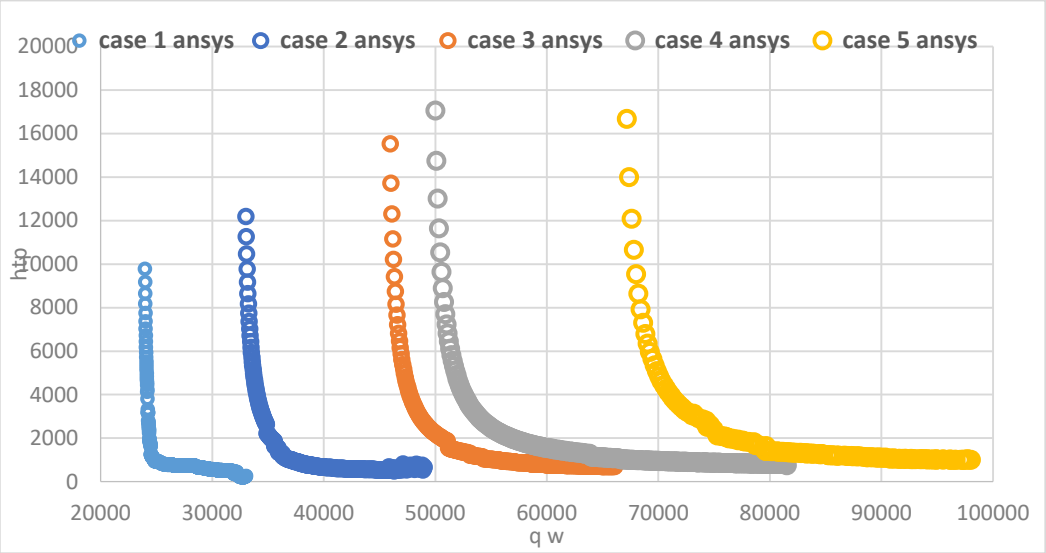

Figure 14 Heat transfer coefficient with heat flux of numerical work.

4.2.2. Void fraction (x) and mass flux

As indicated in Figure 15, for heat flux (33kW/m^2), vapor quality 0.09, and for mass flux 1.63kg/$m^2.s$, the heat transfer coefficient was 9.5 kW/m^2℃ . And for the heat transfer coefficient 20kW/m^2 ℃ , the mass flux was increased up to 8.16 kg/$m^2 s$. However, for a mass flux constant the vapor, quality rises with increasing heat flux when. The heat transfer coefficient can be reduced with increasing heat flux because of decreasing heat transfer with increasing vapour quality. This trend does not support that heat transfer coefficient rises with increasing heat flux. Qu and Mudawer (2003) [6] and Balasubramanian et al. (2013) [11] showed that the heat transfer coefficient increased with the rise of mass flux but reduced with an increase in the vapour quality. Then, for the saturated region in present work, the forced convection boiling is the dominant mechanism. Moreover, Figure 15 demonstrates that the dropping of heat transfer coefficient with increasing vapour quality.

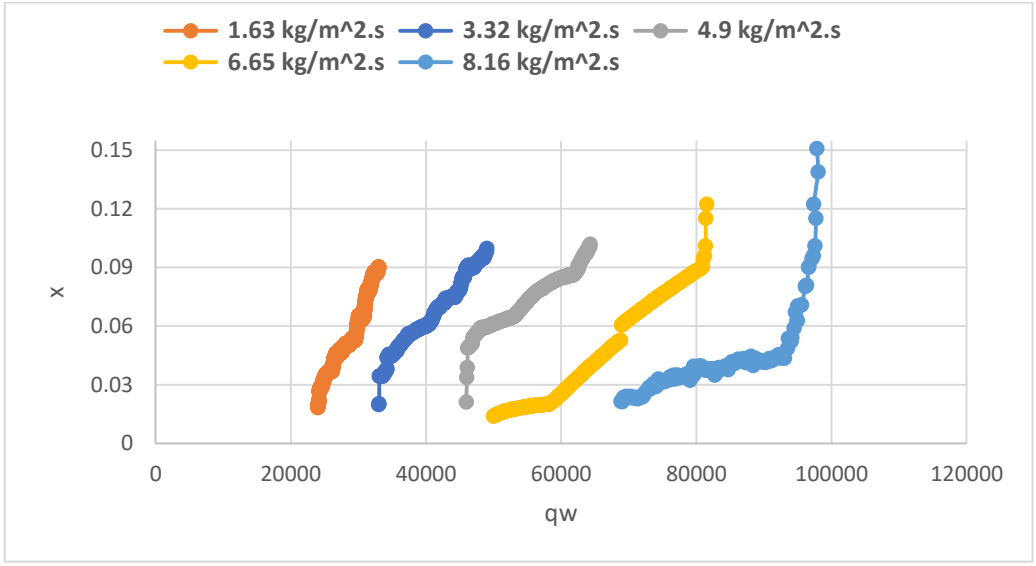

Figure 15 X vapour quality with heat flux of numerical work.

4.3. The effect of Heat flux on the wall temperature

At ONB induces a high releases of latent heat of water and reduces the high degrees of wall temperature that occurs before ONB. Then the temperature rises again with an increase in heat flux where bubbles continues to grow. In reverse flow and dry out the wall temperature rises as high as possible, then drops suddenly due to fluctuation as shown in Figure 13.

4.4. Flow boiling pressure drop

Pressure loss in is one of the most significant parameter in the micro channel design. Figure (10) illustrates the variation of pressure drop with the wall heat flux. It is shown that the rises in the wall heat flux lead to the increase in the pressure drop. However, it was shown that the point of minimum pressure drop does not coincide with the ONB exactly. Where the bubbles elongate and coalesce together and annular flow dominant results in rising of pressure drop. Furthermore, the increasing mass flux from (1.63 -8.16) kg/$m^2 s$ as seen in Figure 16, Figure 17, and Figure 18, increasing pressure drop, this referred that the pressure drop is dependent on the mass flux.

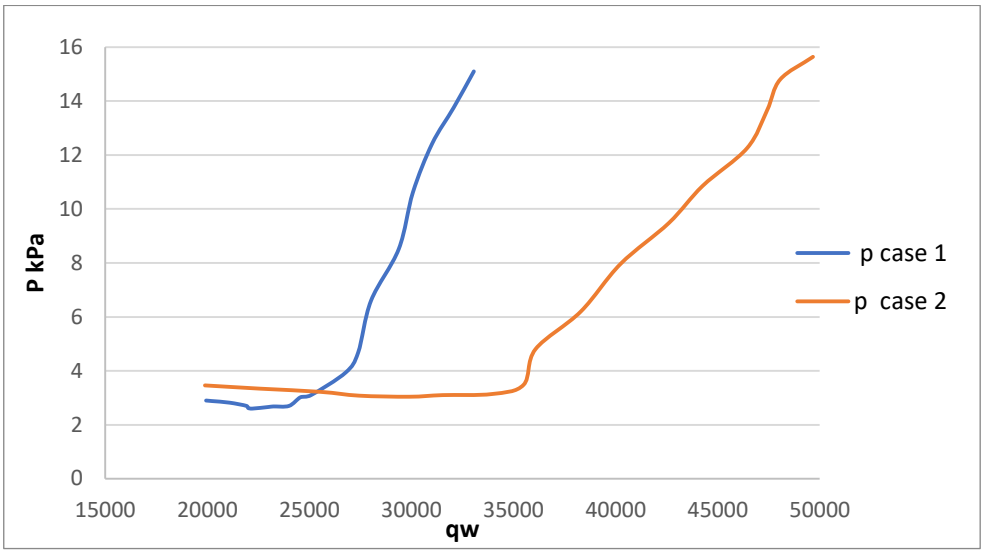

Figure 16 X Pressure drop versus heat flux for various mass flux at 1.63kg/$m^2.s$ and 3.32 kg/$m^2.s$

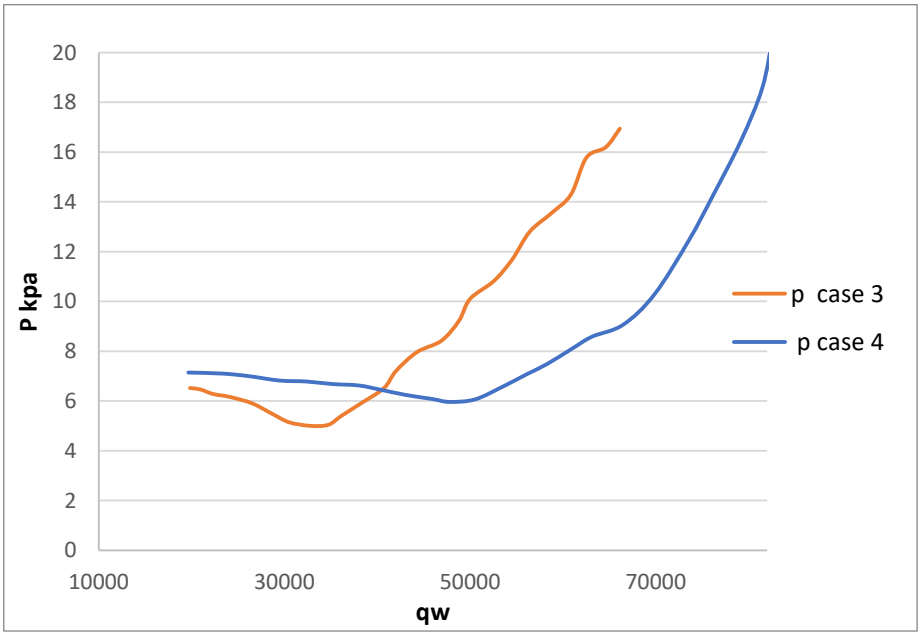

Figure 17 X Pressure drop versus heat flux for various mass flux at 4.9kg/$m^2.s$ and 6.65 kg/$m^2.s$

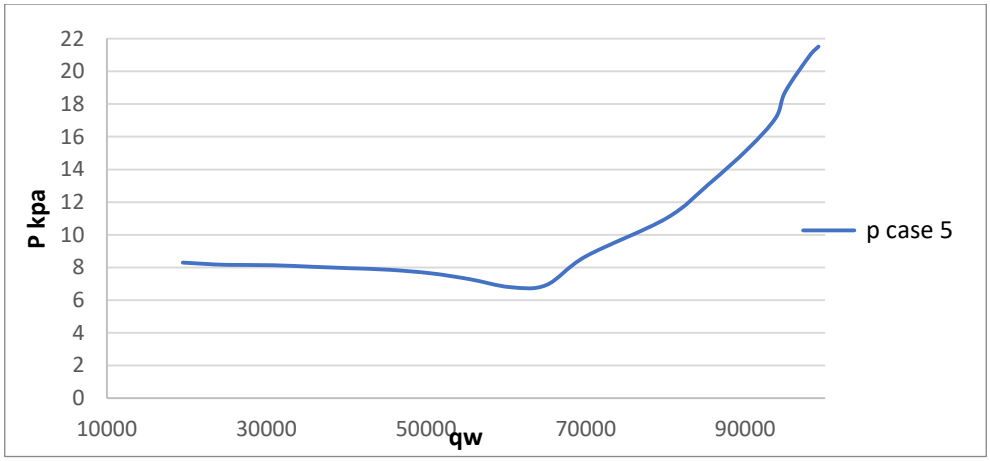

Figure 18 Pressure drop versus heat flux and mass flux at 8.16kg/$m^2.s$

5. CONCLUSIONS

It was concluded that:

1. Flow patterns which were noticed for all cases studied along the channel were: nucleate bubble, bubble flow, slug flow, churn flow and annular flow.
2. An instability was noticed due to a reversed flow which causes by the dryout conditions. For the mass fluxes 1.63 kg/m^2s, 3.32kg/m^2s, 4.9kg/m^2s, 6.65kg/m^2s, and 8.16kg/m^2s, the heat fluxes of ONB and start dryout are 24.8kW/m^2, 33.28kW/m^2, 46.138kW/m^2, 518kW/m^2, and 698kW/m^2 and 33.3 kW/m^2, 50 kW/m^2, 66.7 kW/m^2, 83.3 kW/m^2, and 100 kW/m^2 respectively. Each dryout heat flux causes an oscillation of pressure and temperature.
3. Dry out is an undesirable phenomenon that causes increase wall temperature up to 120℃.
4. Heat transfer coefficient increased with increase mass flux but decreased with an increase vapour quality.
5. The dominant mechanism for saturated region in present work is the forced convection boiling.
6. The point of minimum pressure drop does not coincide with the ONB.
7. The rise of mass flux from (1.63 -8.16) kg/$m^2.s$, cause a more pressure drop. Therefore, it is concluded that the pressure drop is strongly dependent on the mass flux.

6. RECOMMENDATIONS

The present study can be extended in order to explore more options and behaviour of two phase flow process through the microchannel. Therefore, the following recommended for the future work:
The effect of the different dimensions on the value of heat transfer and the value of X quality must be studied to see the disturbances that occur when changing the dimensions. Moreover, using different type of fluid rather than water or adding nano-material to its effect on flow during water nucleation. The use of a variable inlet conditions to the duct with a rate of speed to delay the steam formation process to see its effect on the time taken to reach the dry out state. Furthermore, Conduct an extended study of vertical flow for upward flow and down word flow.

REFERENCES

1. Tuckerman, D., & Pease, R. (1981, May). High-performance heat sinking for VLSI. I*EEE Electron Device Letters*, **2**(5), 126–129. https://doi.org/10.1109/edl.1981.25367.
2. Keyes, R. (1975). Physical limits in digital electronics. *Proceedings of the IEEE*, **63**(5), 740–767. https://doi.org/10.1109/proc.1975.9825.
3. Kandlikar, S. G. (1998, May 1). Heat Transfer Characteristics in Partial Boiling, Fully Developed Boiling, and Significant Void Flow Regions of Subcooled Flow Boiling. *Journal of Heat Transfer*, **120**(2), 395–401. https://doi.org/10.1115/1.2824263.

4. Thome, J. R. (2018, May 20). Encyclopedia of Two-Phase Heat Transfer and Flow III: Macro And Micro Flow Boiling and Numerical Modeling Fundamentals (A 4-volume Set). World Scientific Publishing Co Pte Ltd.
5. Ghiaasiaan, M. S. (2017, January 11). Two-Phase Flow, Boiling, and Condensation: In Conventional and Miniature Systems (2nd ed.). Cambridge University Press.
6. Qu, W., & Mudawar, I. (2003, July). Measurement and prediction of pressure drop in two-phase micro-channel heat sinks. *International Journal of Heat and Mass Transfer*, **46**(15), 2737–2753. https://doi.org/10.1016/s0017-9310(03)00044-9.
7. Lee, J., & Mudawar, I. (2005, February). Two-phase flow in high-heat-flux micro-channel heat sink for refrigeration cooling applications: Part II—heat transfer characteristics. *International Journal of Heat and Mass Transfer*, **48**(5), 941–955. https://doi.org/10.1016/j.ijheatmasstransfer.2004.09.019.
8. Huh, C., & Kim, M. H. (2007, August). Pressure Drop, Boiling Heat Transfer and Flow Patterns during Flow Boiling in a Single Microchannel. *Heat Transfer Engineering*, **28**(8–9), 730–737. https://doi.org/10.1080/01457630701328213.
9. Soupremanien, U., Person, S. L., Favre-Marinet, M., & Bultel, Y. (2011, July). Influence of the aspect ratio on boiling flows in rectangular mini-channels. *Experimental Thermal and Fluid Science*, **35**(5), 797–809. https://doi.org/10.1016/j.expthermflusci.2010.06.014.
10. Galvis, E. & University of Waterloo. Department of Mechanical and Mechatronics Engineering. (2012). Single-phase and Boiling Flow in Microchannels with High Heat Flux. Amsterdam University Press.
11. Balasubramanian, K., Jagirdar, M., Lee, P., Teo, C., & Chou, S. (2013, November). Experimental investigation of flow boiling heat transfer and instabilities in straight microchannels. *International Journal of Heat and Mass Transfer*, **66**, 655–671. https://doi.org/10.1016/j.ijheatmasstransfer.2013.07.050.
12. Fayyadh, E., Mahmoud, M., Sefiane, K., & Karayiannis, T. (2017, July). Flow boiling heat transfer of R134a in multi microchannels. *International Journal of Heat and Mass Transfer*, **110**, 422–436. https://doi.org/10.1016/j.ijheatmasstransfer.2017.03.057.
13. Yin, L., Xu, R., Jiang, P., Cai, H., & Jia, L. (2017, September). Subcooled flow boiling of water in a large aspect ratio microchannel. *International Journal of Heat and Mass Transfer*, **112**, 1081–1089. https://doi.org/10.1016/j.ijheatmasstransfer.2017.05.028.
14. Kuang, Y., Wang, W., Miao, J., Yu, X., Zhang, H., & Zhuan, R. (2017, February). Flow boiling of ammonia and flow instabilities in mini-channels. *Applied Thermal Engineering*, **113**, 831–842. https://doi.org/10.1016/j.applthermaleng.2016.11.093.
15. Al-Nakeeb, Q. A., Fayyadh, E. M., & Hasan, M. R. (2021, February 1). Experimental Investigation of Sub-Cooled Flow Boiling Heat Transfer in Single Rectangular Metallic Micro-Channel. *IOP Conference Series: Materials Science and Engineering*, **1094**(1), 012056. https://doi.org/10.1088/1757-899x/1094/1/012056.
16. Özdemir, M. R., Mahmoud, M. M., & Karayiannis, T. G. (2020, January 25). Flow Boiling of Water in a Rectangular Metallic Microchannel. *Heat Transfer Engineering*, **42**(6), 492–516. https://doi.org/10.1080/01457632.2019.1707390.

17. Cuan, Z., & Chen, Y. (2017). Analyze of laminar flow and boiling heat transfer characteristics of R134a in the horizontal micro-channel under low temperature condition. *Procedia Engineering*, **205**, 2933–2939. https://doi.org/10.1016/j.proeng.2017.10.106.
18. LIU, Q. (2017). Numerical study of flow boiling in micro/mini channels (Doctoral thesis 2017). Department of Energy Technology School of Industrial Engineering and Management KTH Royal Institute of Technology SE 100-44 Stockholm.
19. Al-Waaly, A. (2015). The effect of heat transfer on temperature measurement and it's applications to study microchannel heat sinks. In PhD thesis. University of Glasgow, Glasgow, UK.
20. Moffat, R. J. (1988, January). Describing the uncertainties in experimental results. *Experimental Thermal and Fluid Science*, **1**(1), 3–17. https://doi.org/10.1016/0894-1777(88)90043-x.
21. Ansys Software user guide, 2021. (2021). In Ansys. ANSYS, Inc.January 2021Southpointe2600 ANSYS DriveCanonsburg, PA 15317.

NOMENCLATURE

Symbol	Definition	Units(SI)
A_s	Channel surface area	m^2
L	Length	m
W	Width	m
T	Thickness	m
ρ	Density	kg/m^3
g	Acceleration gravity	m/s^2
h	Height	m
p	Pressure	Pa
Tw	Wall temperature	^oC
q_w	Heat flux	kW/m^2
h_{tp}	Heat transfer coefficient	kW/m^2 ℃
x	Void fraction	
ONB	Onset nucleate boiling	
CFD	Computational Fluid Dynamics	